atmosphere

MDPI

Article

Assessing the Effectiveness of Spectral Nudging in Improving Tropical Cyclone Track Simulations over the Western North Pacific Using the WRF Model

Weiwei Huang [1], Lian Xie [2,*], Fei Hong [1] and Jiwen Zhu [1]

[1] Beijing Fengyun Meteorological Science and Technology Development Co., Ltd., Beijing 100081, China; huangww@cma.gov.cn (W.H.); hongfei@fengyun.work (F.H.); zhujiwen@fengyun.work (J.Z.)
[2] Department of Marine, Earth and Atmospheric Sciences, North Carolina State University, Box 8208, Raleigh, NC 27695-8208, USA
* Correspondence: xie@ncsu.edu

Abstract

Improving tropical cyclone (TC) track forecasts is critical for enhancing disaster prevention and mitigation efforts. This study evaluates the effectiveness of the spectral nudging (SN) technique in simulating TC tracks with diverse path patterns over the Western North Pacific using the Weather Research and Forecasting (WRF) model. The results show that the SN technique is remarkably effective in improving tropical cyclone track forecasts for all types of regular track patterns, except for irregular tracks. Specifically, spectral nudging reduced simulated mean track position errors by approximately 60%, 67%, and 77% on average for curving, northwestward-, and westward-moving tracks, respectively. Better simulations of large-scale flow dynamics contributed to these improvements, particularly in scenarios where the subtropical high underwent rapid changes in its circulation patterns. For irregular tracks, applying the SN technique showed mixed results, ranging from 75% error reduction to 20% error increase. This implies that the effectiveness of spectral nudging on the simulation of irregular tracks is case dependent. Since the effectiveness of spectral nudging depends on the scales (spectrum) of the underlying processes creating the irregularities of the tracks, when such irregularities were caused by local and regional-scale factors, spectral nudging became ineffective.

Keywords: spectral nudging; TC simulation; WRF model; TC track patterns

check for updates

Academic Editor: Corene Matyas

Received: 10 July 2025
Revised: 18 August 2025
Accepted: 29 August 2025
Published: 30 August 2025

Citation: Huang, W.; Xie, L.; Hong, F.; Zhu, J. Assessing the Effectiveness of Spectral Nudging in Improving Tropical Cyclone Track Simulations over the Western North Pacific Using the WRF Model. *Atmosphere* **2025**, *16*, 1028. https://doi.org/10.3390/atmos16091028

Copyright: © 2025 by the authors. Licensee MDPI, Basel, Switzerland. This article is an open access article distributed under the terms and conditions of the Creative Commons Attribution (CC BY) license (https://creativecommons.org/licenses/by/4.0/).

1. Introduction

Tropical cyclones are responsible for high winds, heavy rainfall, storm surges, and secondary disasters such as floods and landslides. These events collectively cause more significant economic and human losses globally than earthquakes, tsunamis, and volcanic eruptions [1–3]. Approximately one-third of all tropical cyclones originate in the western North Pacific Ocean, making it the most active tropical cyclone basin worldwide [1]. Accurate prediction of tropical cyclone tracks supports government efforts to prepare for, mitigate, and assess the impact of these disasters [4].

The 1990s saw the emergence of many new Numerical Weather Prediction (NWP) models, including both global and regional limited-area models (LAMs). These advances established NWP as a primary method for forecasting tropical cyclone paths, particularly with the improved understanding of the physics governing tropical cyclone movement in the Western North Pacific (WNP) basin [5–7]. Global models excel at simulating large-scale

circulation, a key determinant of tropical cyclone tracks [8], while high-resolution LAMs are more effective at capturing the small-scale features of tropical cyclones. However, conventional lateral boundary nesting approaches sometimes distort information transferred from global models to LAMs [9].

To mitigate accumulated errors in large-scale circulation within the boundary sponge region and the integration area of LAMs, the spectral nudging technique has often been employed. This method adjusts the large-scale solution in the LAM toward the global forcing while allowing the LAM to develop its small- and regional-scale dynamics independently [10–12]. Over the past 20 years, spectral nudging has been widely used in regional climate dynamical downscaling studies and tropical cyclone track simulations [9,13–16]. However, most studies focused on individual tropical cyclone cases, with limited research on the impact of spectral nudging across various track patterns.

This study aims to evaluate the effectiveness of the spectral nudging technique in simulating tropical cyclone tracks with diverse track patterns over the WNP. Section 2 provides an overview of the spectral nudging method. Section 3 details the model setup and experimental design. Section 4 presents and discusses the results, while Section 5 summarizes the conclusions.

2. Spectral Nudging Technique

The spectral nudging technique integrates time-varying large-scale atmospheric states into a regional atmospheric model, facilitating a more precise simulation of large-scale flows [11]. This approach treats regional numerical simulation as a downscaling problem, where the method ensures the regional model adheres not only to boundary conditions but also to large-scale flow conditions within the integration area [10–12]. Considered a suboptimal and indirect data assimilation method, spectral nudging introduces an additional term to the tendencies of model variables. This term relaxes the selected portion of a spectrum to align with corresponding waves from analysis or reanalysis data or global model predictions, enabling the regional model to closely replicate large-scale components. Moreover, the nudging term is applied only to large-scale flows at higher altitudes, allowing the regional model to develop more freely near the surface [11].

The mathematical representation of this technique begins with the expansion of a regional model variable (Ψ):

$$\Psi(\lambda, \phi, t) = \sum_{j=-J_m, k=-K_m}^{J_m, K_m} \alpha_{j,k}^{m}(t) \exp(ij\lambda/L_\lambda) \exp(ik\phi/L_\phi) \quad (1)$$

Here, λ represents zonal coordinates, j denotes zonal wavenumbers, and L_λ is the zonal extension of the area. Similarly, ϕ represents meridional coordinates, k denotes meridional wavenumbers, and L_ϕ is the meridional extension. The variable t denotes time, while J_m and K_m represent the highest zonal and meridional wavenumbers, respectively, for the regional model. Typical variables subjected to this expansion include horizontal wind components (u, v), temperature (T), and geopotential height (Φ) [11].

A similar expansion applies to analyses, which are based on a coarser grid:

$$\Psi_a(\lambda, \phi, t) = \sum_{j=-J_a, k=-K_a}^{J_a, K_a} \alpha_{j,k}^{a}(t) \exp(ij\lambda/L_\lambda) \exp(ik\phi/L_\phi) \quad (2)$$

Here, $\alpha_{(j,k)}^{a}$ represents the coefficients of the analyses, with the number of Fourier coefficients satisfying $J_a < J_m$ and $K_a < K_m$. The nudging terms are then calculated as:

$$\sum_{j=-J_a, k=-K_a}^{J_a, K_a} \eta_{j,k} \left[\alpha_{j,k}^{a}(t) - \alpha_{j,k}^{m}(t)\right] \exp(ij\lambda/L_\lambda) \exp(ik\phi/L_\phi) \quad (3)$$

In this expression, $\eta_{(j,k)}$ is a confidence coefficient that reflects the realism of the analyses at different scales, depending on the wavenumbers J and K. The value of $\eta_{(j,k)}$ increases with altitude, implying greater confidence in the analyses and more effective nudging at higher altitudes.

The complete spectral nudging equation is formulated as:

$$\frac{\partial \Psi}{\partial t} = L(\Psi) - \sum_{j=-J_a,k=-K_a}^{J_a,K_a} \eta_{j,k}\left[\alpha_{j,k}^{a}(t) - \alpha_{j,k}^{m}(t)\right]\exp(ij\lambda/L_\lambda)\exp(ik\phi/L_\phi) \quad (4)$$

Here, L denotes the model operator [15]. By employing the spectral nudging technique, specific model variables can be selectively constrained to align with reanalysis data or global model prediction at specific scales or altitudes, enhancing the simulation's overall accuracy.

3. Model Setup and Experiment Design

This study employs the Weather Research and Forecasting (WRF) model (version 4.0) with the Advanced Research WRF (ARW) core [17], designed to solve fully compressible, Eulerian non-hydrostatic equations. The WRF model features a terrain-following, mass-based hybrid sigma-pressure vertical coordinate system based on dry hydrostatic pressure, allowing vertical grid stretching and terminating at a constant pressure surface. Its horizontal structure uses an Arakawa C-grid staggering, with time-split integration achieved through second- or third-order Runge–Kutta schemes, employing smaller time steps for acoustic and gravity wave modes.

The model incorporates various physical processes, including microphysics, cumulus parameterization, planetary boundary layer (PBL), surface layer, land surface, and longwave and shortwave radiation, with multiple options for each process. Spectral nudging, implemented in the WRF ARW since 2010, applies to variables u, v, temperature, and geopotential height, while spectral nudging for the moisture mixing ratio was also introduced in version 4.0.

The National Centers for Environmental Prediction (NCEP) Final (FNL) operational model global tropospheric analysis data provides initial and lateral boundary conditions in this study. These analyses are produced on a $1^\circ \times 1^\circ$ grid at 6 h intervals. The FNL data, developed using the same model as NCEP's Global Forecast System (GFS), assimilates a broader range of observations, including those from the Global Telecommunications System (GTS), resulting in reliable large-scale flow representation. However, finer-scale features may be poorly represented due to the coarse grid resolution.

To evaluate the effectiveness of spectral nudging in tropical cyclone (TC) track simulations, control (CTL) and spectral nudging (SN) sensitivity experiments were conducted for each TC case. Results were output at 2 h intervals. Table 1 outlines the configuration used in the WRF model. The model domain, with terrain height in meters for TC simulations, is shown in Figure 1.

Twenty-nine TCs over the Western North Pacific (WNP) from 2005 to 2019 were selected to evaluate the spectral nudging technique's performance and sensitivity in simulating different TC track patterns. These patterns were classified into four categories:

1. Type 1: West–northwest–north curving tracks passing north of Taiwan (referred to as curving tracks, hereafter).
2. Type 2: Northwestward tracks passing near Taiwan.
3. Type 3: Westward tracks passing south of Taiwan.
4. Type 4: Irregular tracks.

Table 1. Description of model configurations.

Description	Selection
WRF version	4.0
Dynamic solver	ARW
Horizontal grid spacing	36 km
Vertical levels	45 (top 50 hPa)
Integration time	120 s
Microphysics	WSM6
Longwave radiation	RRTMG
Shortwave radiation	RRTMG
Surface	Revised MM5 Monin–Obukhov
Land surface	NOAH
Planetary boundary layer	YSU
Cumulus parameterization	Tiedtke
Initial and boundary data	NCEP FNL 1.0° × 1.0°, every 6 h, with a 6 h boundary update
Geographical data	USGS 30″ DEM (terrain), USGS 24-category 30″ (land use), default green fraction/albedo/soil type from WPS_GEOG
Spin-up	12 h (not included in evaluation period)

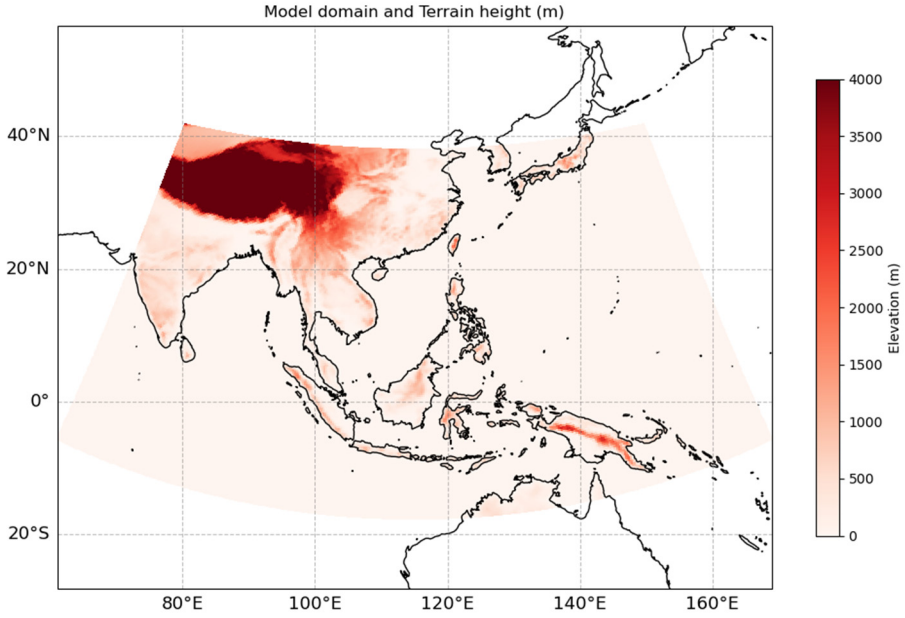


Figure 1. Model domain with terrain elevation in meters for TC simulations.

The CTL and SN experiments used identical model configurations, differing only in the application of spectral nudging. CTL experiments excluded spectral nudging, while SN sensitivity tests implemented spectral nudging using specific wavenumbers tailored to each TC's domain. The WRF model utilized a horizontal grid spacing of 36 km, being roughly 1/3 of the FNL resolution (1° × 1°, approximately 111 km at the equator), which provided sufficient detail to capture the large-scale circulation patterns. Approximately nine grids of FNL data were needed to represent a large-scale wave adequately, allowing the FNL analysis to resolve waves with lengths of approximately 900 km or longer. Ja and Ka represent the maximum wavenumbers (truncation wavenumbers) for nudging, where Ja denotes the zonal wavenumber and Ka denotes the meridional wavenumber.

Most TC simulation domains were in lower-latitude regions, where wind predominates over pressure during the initial stages of a TC's lifecycle. Mid-tropospheric winds

(500–700 hPa) within a radius of 5–7° latitude from the cyclone center demonstrated the strongest correlation with TC movement [8]. Consequently, horizontal wind components (u and v) were selected as spectral nudging variables. Regarding the levels, spectral nudging was applied to the whole vertical levels throughout the simulation periods. The nudging coefficient for u and v was set to 0.0003 s^1, a default setting in SN runs. This setup ensures that large-scale wind patterns, which dominate TC steering flows across different altitudes, are constrained to align with the reanalysis data while allowing small-scale dynamics to develop freely as needed. Several cases of Type 2 and Type 3 were randomly selected, with the values of Ja and Ka adjusted upward or downward slightly to test their sensitivity. Table 2 details the experimental setup for the selected TCs.

Table 2. SN sensitivity experiment details. For some case tests, there are two setups of wavenumbers, representing SN and SN1.

Typhoon Cases	Track Patterns	Wavenumbers
Ampil 2018	Type 1	Ja = 6, Ka = 9
Haikui 2012	Type 1	Ja = 7, Ka = 6
Lekima 2019	Type 1	Ja = 5, Ka = 6
Matsa 2005	Type 1	Ja = 7, Ka = 10
Meari 2011	Type 1	Ja = 6, Ka = 9
Mitag 2019	Type 1	Ja = 8, Ka = 9
Muifa 2011	Type 1	Ja = 7, Ka = 10
Rumbia 2018	Type 1	Ja = 7, Ka = 6
Haitang 2005	Type 2	Ja = 11, Ka = 7
Soulik 2013	Type 2	Ja = 9, Ka = 5
Nepartak 2016	Type 2	Ja = 7, Ka = 5 (SN) Ja = 8, Ka = 6 (SN1)
Meranti 2016	Type 2	Ja = 7, Ka = 5 (SN) Ja = 7, Ka = 0 (SN1)
Saola 2012	Type 2	Ja = 7, Ka = 6 (SN) Ja = 8, Ka = 7 (SN1)
Talim 2005	Type 2	Ja = 7, Ka = 5
Matmo 2014	Type 2	Ja = 7, Ka = 9 (SN) Ja = 6, Ka = 8 (SN1)
Longwang 2005	Type 2	Ja = 8, Ka = 9
Dujuan 2015	Type 2	Ja = 7, Ka = 5 (SN) Ja = 8, Ka = 6 (SN1)
Usagi 2013	Type 2	Ja = 8, Ka = 6
Trami 2013	Type 2	Ja = 7, Ka = 6
Soudelor 2015	Type 2	Ja = 7, Ka = 5 (SN) Ja = 8, Ka = 6 (SN1)
Megi 2016	Type 2	Ja = 7, Ka = 5 (SN) Ja = 8, Ka = 6 (SN1)
Damrey 2005	Type 3	Ja = 8, Ka = 6
Haiyan 2013	Type 3	Ja = 10, Ka = 6

Table 2. *Cont.*

Typhoon Cases	Track Patterns	Wavenumbers
Mangkut 2018	Type 3	Ja = 10, Ka = 6 (SN) Ja = 10, Ka = 5 (SN1)
Rammasun 2014	Type 3	Ja = 10, Ka = 5
Utor 2013	Type 3	Ja = 7, Ka = 6
Ewiniar 2018	Type 4	Ja = 5, Ka = 5
Megi 2010	Type 4	Ja = 7, Ka = 5
Vicente 2012	Type 4	Ja = 7, Ka = 6

The simulation results from CTL and SN experiments were compared with the best track data available in the China Meteorological Administration's tropical cyclone database [18].

4. Results

4.1. Quantitative Assessment of Tropical Cyclone Track Forecast Errors

In this study, the mean absolute track position error (TPE) is used as the quantitative estimation of TC track error. The TPE (in km) is defined as the great circle distance between the storm location in the best track data and the simulated storm center valid at the same time averaged over the sampling period [9]. Table 3 provides the simulated TC track position errors for each case. The overwhelming majority of the simulated TPE for the SN and SN1 simulations were smaller than those for the CTL, showing small adjustments to the cutoff wavenumbers in the nudging process create little impact on the track simulations. However, setting only the zonal wavenumber while keeping the meridional wavenumber at 0 led to a significant increase in track TPE for Typhoon Meranti (2016).

Table 3. Simulated tropical cyclone track position errors (TPEs) for the set of experiments: CTL, SN, and SN1.

Track Type	Typhoon Cases	Track Position Errors (km)		Improvement (%)
		CTL	SN/SN1	(CTL−SN)/CTL
1	Ampil 2018	198.30	85.74 *	56.8
1	Haikui 2012	235.65	43.83 *	81.4
1	Lekima 2019	431.45	49.97 *	88.4
1	Matsa 2005	116.88	72.74 *	37.8
1	Meari 2011	110.96	79.65 *	28.2
1	Mitag 2019	136.28	74.83 *	45.1
1	Muifa 2011	357.51	26.27 *	92.7
1	Rumbia 2018	172.04	89.24 *	48.1
2	Haitang 2005	297.27	57.50 *	80.7
2	Soulik 2013	129.28	39.30 *	69.6
2	Nepartak 2016	216.51	44.10 */41.58 *	79.6/80.8
2	Meranti 2016	211.75	50.34 */453.16 *	76.2/−114
2	Saola 2012	239.49	68.60 */49.86 *	71.4/79.2
2	Talim 2005	277.91	60.12 *	78.4
2	Matmo 2014	193.34	72.53 */73.53 *	62.5/62.0

Table 3. *Cont.*

Track Type	Typhoon Cases	Track Position Errors (km)		Improvement (%)
		CTL	SN/SN1	(CTL−SN)/CTL
2	Longwang 2005	715.03	81.70 *	88.6
2	Dujuan 2015	172.81	43.14 */48.10 *	75.0/72.2
2	Usagi 2013	44.74	16.87 *	62.3
2	Trami 2013	165.54	49.57 *	70.1
2	Soudelor 2015	52.02	31.82 */30.70 *	38.8/41.0
2	Megi 2016	218.75	174.94 */150.93 *	20.0/31.0
3	Damrey 2005	112.85	45.53 *	59.7
3	Haiyan 2013	158.72	28.24 *	82.2
3	Mangkut 2018	134.05	26.13 */29.75 *	80.5/77.8
3	Rammasun 2014	165.17	43.78 *	73.5
3	Utor 2013	361.72	39.86 *	89.0
4	Ewiniar 2018	63.54	76.20	−19.9
4	Megi 2010	205.22	51.68 *	74.8
4	Vicente 2012	198.80	82.72 *	58.4

The Mann–Whitney U test was employed to determine whether the improvements in TPE by using spectral nudging are statistically significant. The Mann–Whitney U test derives an exact *p*-value for small samples and can detect location differences between two groups without assuming normality [19]. In Table 3, an asterisk (*) indicates that the TPE difference between the CTL and SN/SN1 simulations is statistically significant at the 95% confidence level. Except for Typhoon Ewiniar (2018), the TPEs of SN simulations in all other cases were significantly improved compared with the CTL runs, with TPE reductions between 20% and 92.7% (Table 3).

4.2. West–Northwest–North Curving Track Passing North of Taiwan Island

Simulations using spectral nudging (SN) showed significant improvements in tropical cyclone (TC) track simulations compared to control (CTL) runs in all track types. These improvements were evident in the curving (Type 1) track cases, such as Ampil (2018), Lekima (2019), Meari (2011), Muifa (2011), Mitag (2019) (Figure 2a–f), and Rumbia (2018), a representative TC exhibiting a distinct recurving track over the WNP (Figure 2g). The average TPE reduction is approximately 60% for these Type 1 track cases.

Analysis of the streamlined simulations for CTL and SN runs highlighted typical large-scale flow patterns that contributed to the track errors in the CTL experiments. A notable pattern involved changes in the subtropical high-pressure system from an east–west orientation to a north–south configuration. This transition influenced the storm's steering flow, which the SN simulations accurately reproduced, while the CTL runs failed to capture the pattern change. For instance, in Lekima (2019), the subtropical high over Japan and the Philippine Islands transitioned to a north–south alignment in the SN run, prompting the storm to move northward along the southwestern edge of the high-pressure system over Japan. In contrast, the CTL run depicted the subtropical high-pressure system over the Philippine Islands with an east–west oriented circulation pattern, resulting in a more pronounced zonal deviation of the storm track compared to the best track (Figure 3a,b).

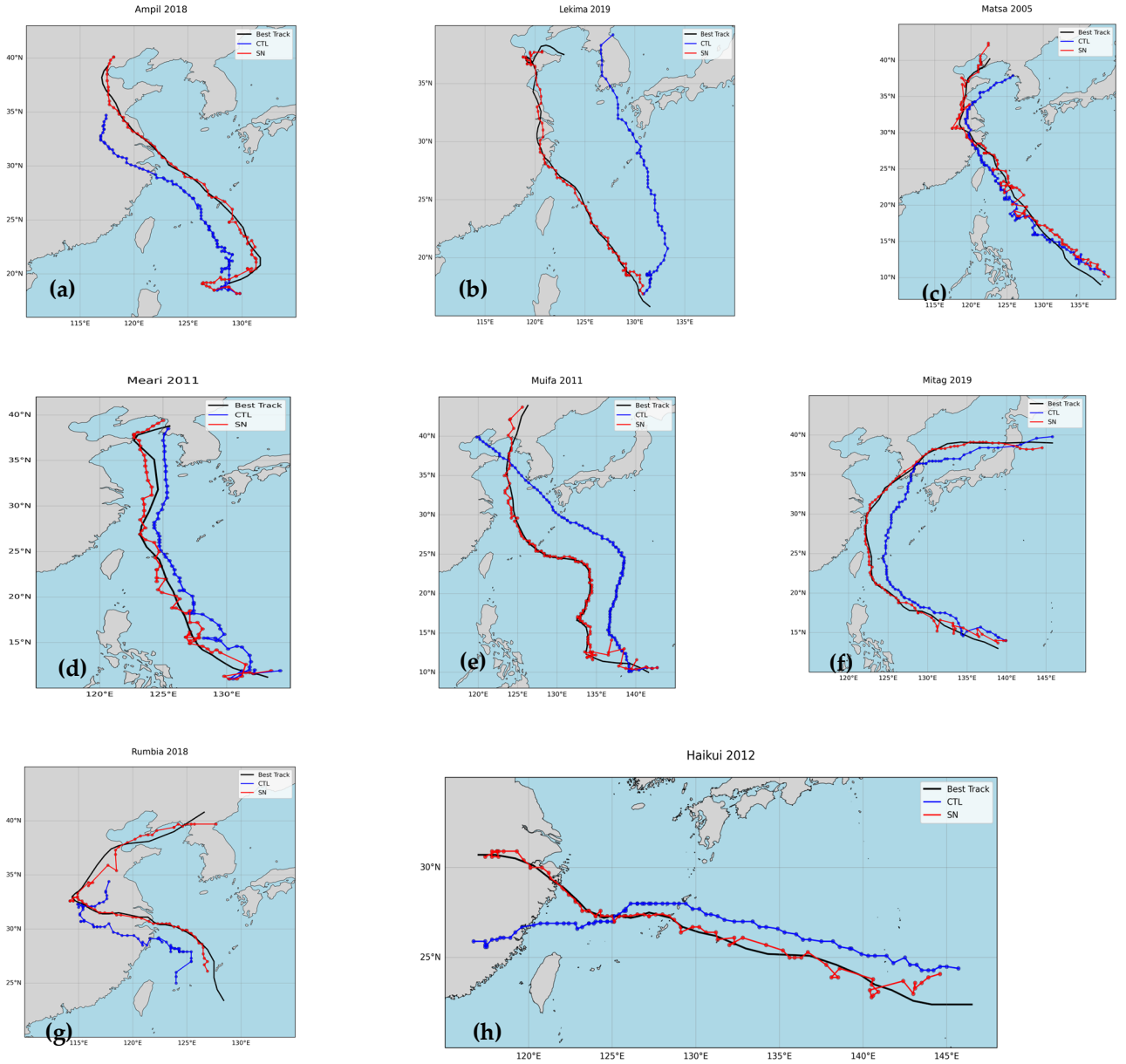


Figure 2. Simulated storm tracks of Type 1 TCs for CTL and SN runs. Black curves represent the best tracks, blue curves represent CTL, and red curves represent SN. (**a**–**h**) Ampil (2018), Lekima (2019), Matsa (2005), Meari (2011), Muifa (2011), Mitag (2019), Rumbia (2018), and Haikui (2012), respectively.

Another key pattern involved the simulation of the north subtropical high (located over Japan), a critical factor for predicting northwest–north curving storm tracks. For Muifa (2011), the SN simulation captured this change, allowing the TC to shift northward under the influence of the merged high-pressure system (Figure 4a,c). In contrast, the CTL run failed to accurately simulate the evolution of the subtropical high, causing the storm to maintain a northwestward trajectory, resulting in a pronounced eastward deviation of the storm track compared to the best track (Figure 4b,d).

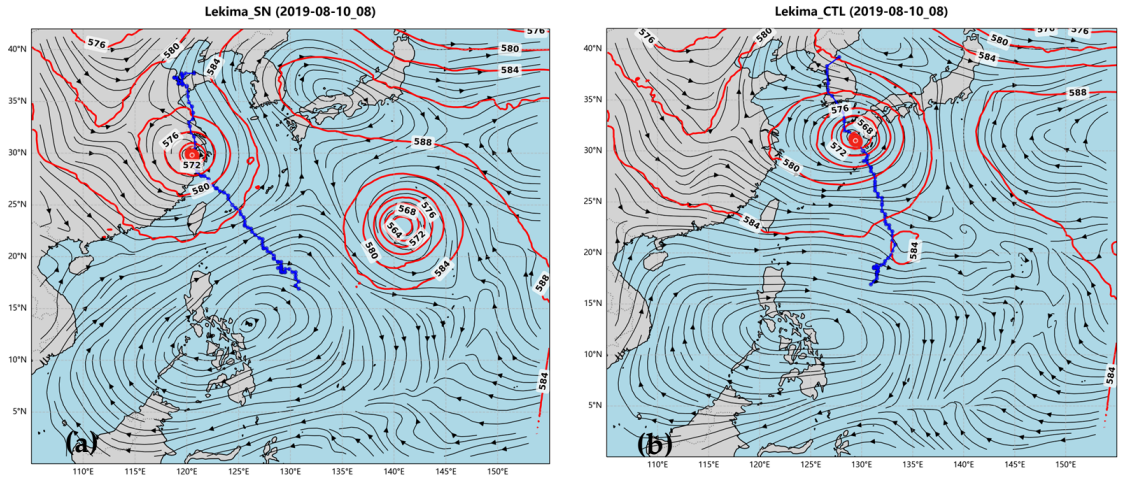


Figure 3. The 500 hPa streamlines for Lekima (2019) simulated by SN (**a**) and CTL (**b**) at 0800 UTC, 10 August 2019. The red symbol marks the storm center.

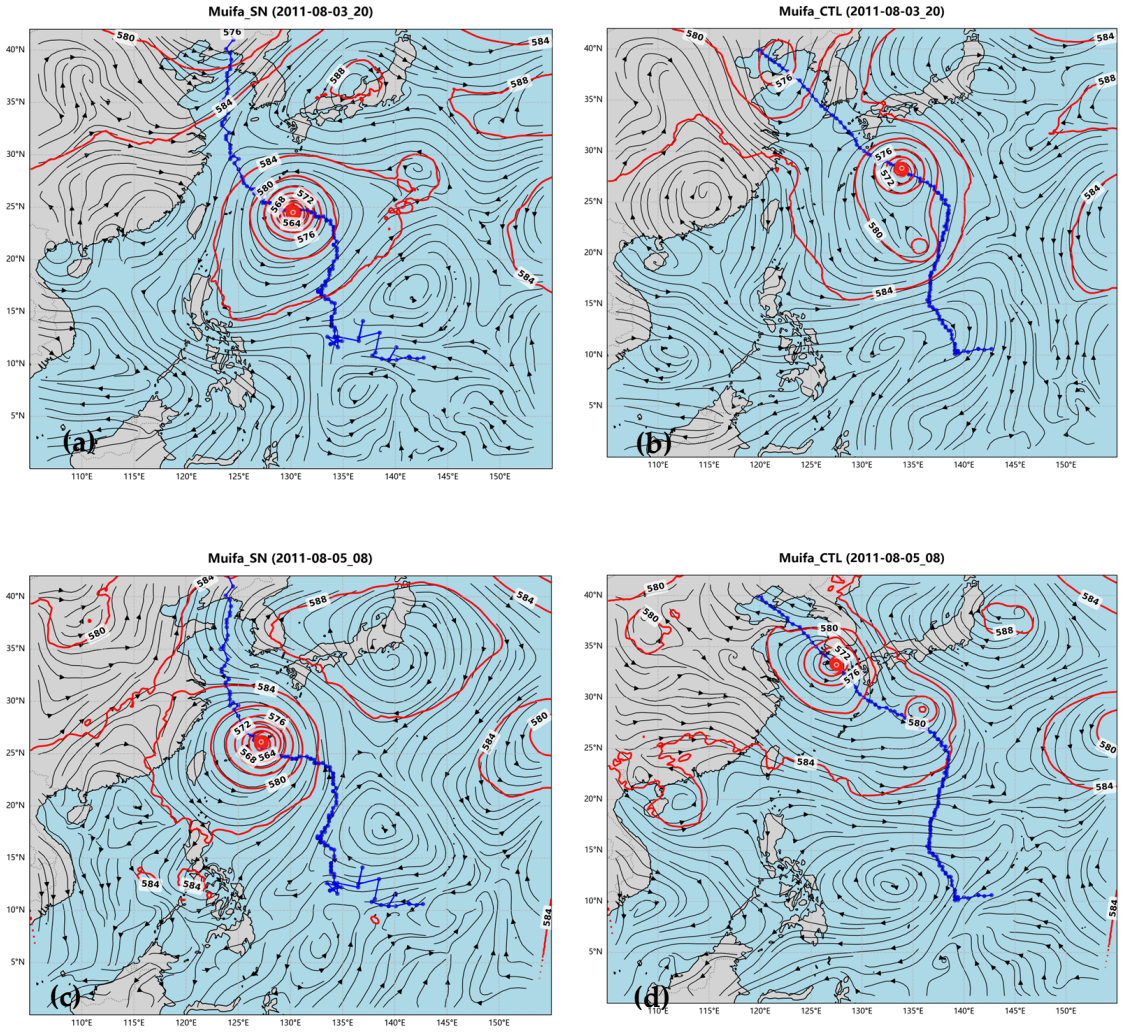


Figure 4. The 500 hPa streamlines for Muifa (2011) simulated by SN (**a**,**c**) and CTL (**b**,**d**) at 2000 UTC, 3 August 2011, and 0800 UTC, 5 August 2011. The red symbol marks the storm center.

In cases where the subtropical high interacted with a westerly trough, significant track errors were observed in the CTL experiments. For Rumbia (2018), the SN simulation successfully captured the TC's track curvature following the extratropical transition into the

midlatitude westerly trough, driven by vortex coupling [20], whereas the CTL run failed to reproduce this dynamic interaction, erroneously depicting a quasi-stationary system over eastern China instead of the observed northward-curving trajectory (Figure 5).

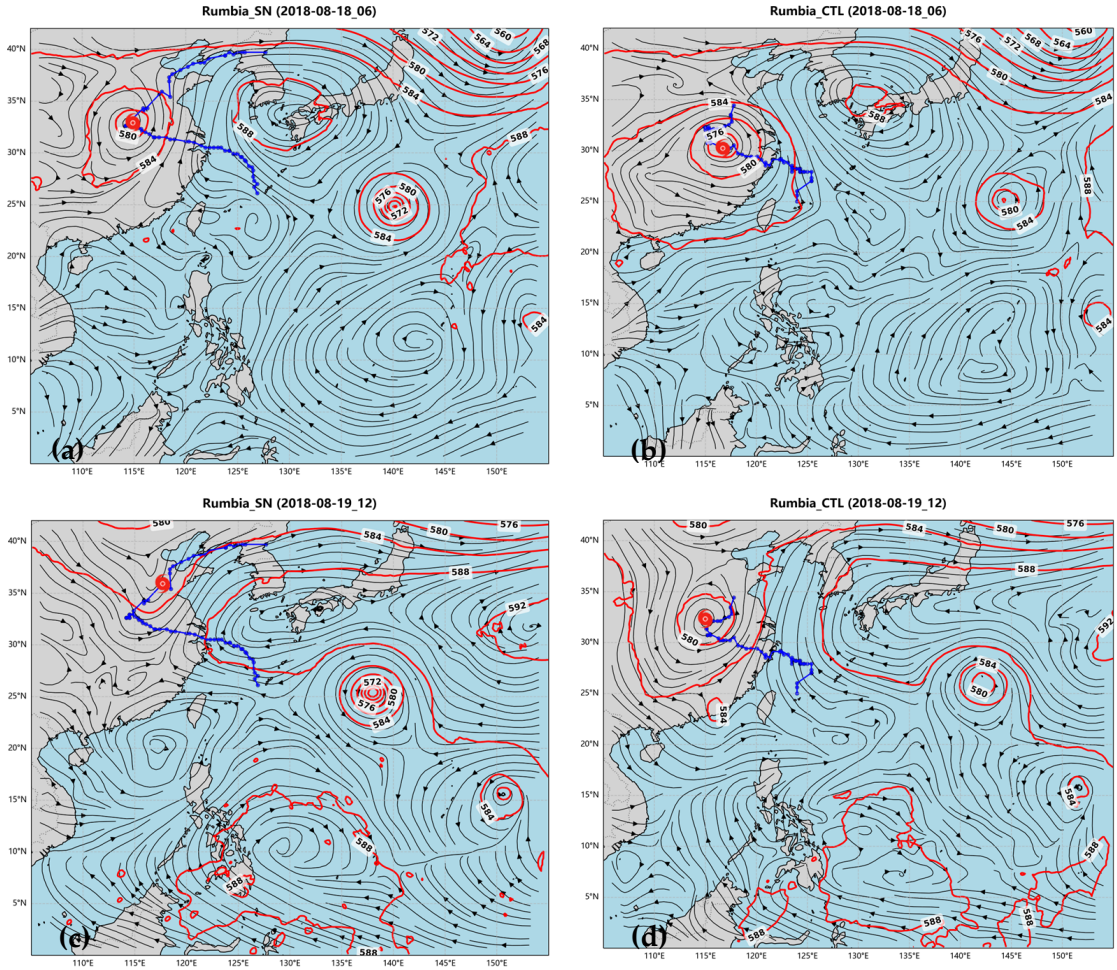


Figure 5. The 500 hPa streamlines for Rumbia (2018) simulated by SN (**a**,**c**) and CTL (**b**,**d**) at 0600 UTC, 18 August 2018, and 1200 UTC, 19 August 2018, respectively. The red symbol marks the storm center.

4.3. Northwest Track Passing Vicinity of Taiwan

The northwest track near Taiwan (Type 2) is a common trajectory over the Western North Pacific (WNP). For this track pattern, 13 TC cases were analyzed. Approximately 75% of the CTL simulations exhibited significant errors, whereas the SN runs consistently outperformed the CTL runs (Figure 6), achieving 67% TPE reduction on average. The SN experiments showed little sensitivity to wavenumber settings (e.g., Figure 6a,c,d,f,g,l), except in cases where the meridional wavenumber was set to zero, leading to larger errors than in the CTL (Figure 6e).

For Type 2 track patterns, TCs were predominantly steered by the subtropical high-pressure systems. Errors in CTL simulations occurred when these systems underwent structural changes, such as breaking into distinct west and east cells, merging of cells, or overestimation of the west cell's intensity. The SN simulations better captured these subtropical high-flow changes, as illustrated in Dujuan (2015) (Figure 7).

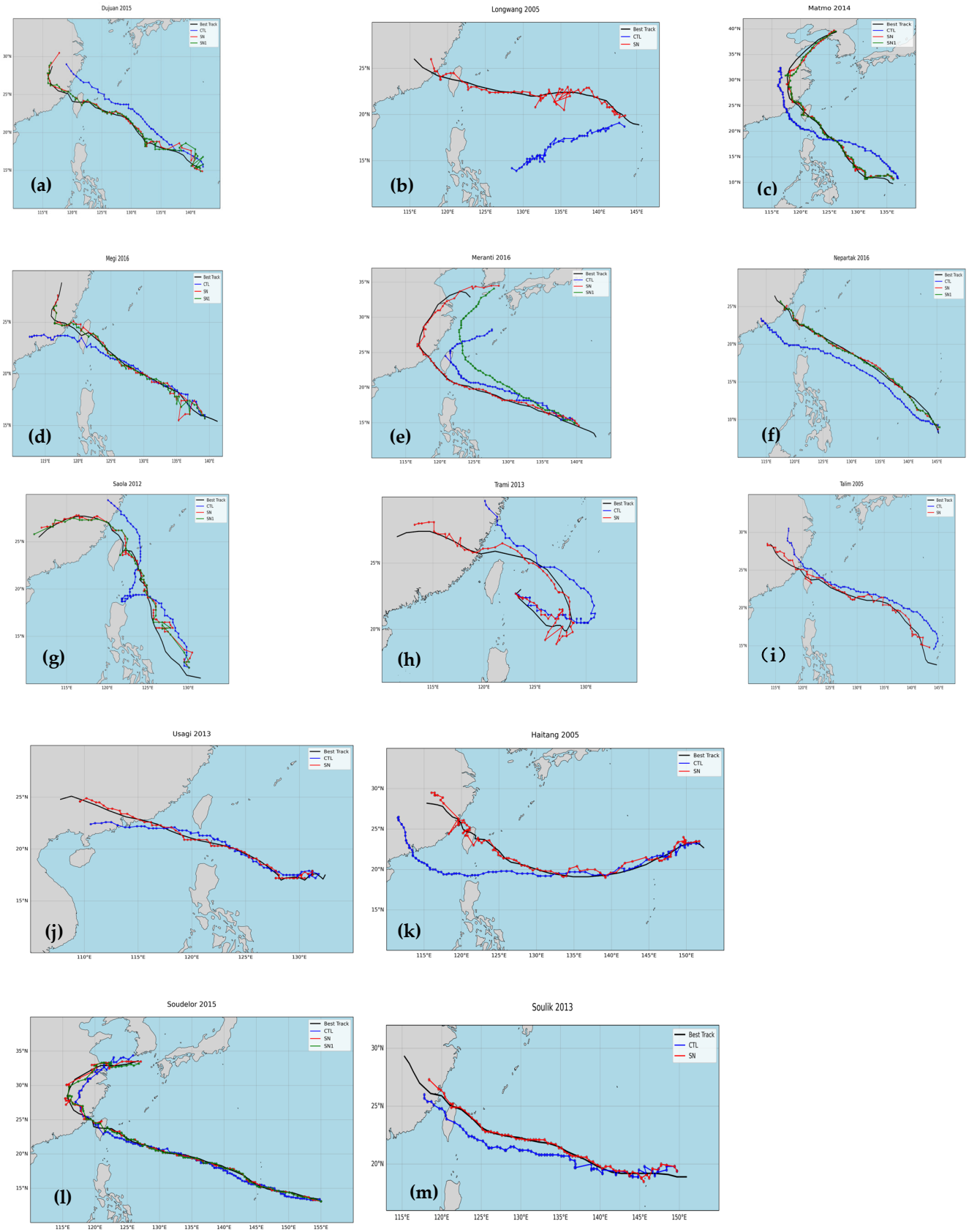


Figure 6. Simulated storm tracks of Type 2 TCs for CTL and SN runs. Black curves represent the best track, blue curves represent CTL, and red and green curves represent SN and SN1, respectively. (**a**–**m**) Dujuan (2015), Longwang (2005), Matmo (2014), Megi (2016), Meranti (2016), Nepartak (2016), Saola (2012), Trami (2013), and Talim (2005), Usagi (2013), Haitang (2005), Soudelor (2015), and Soulik (2013), respectively.

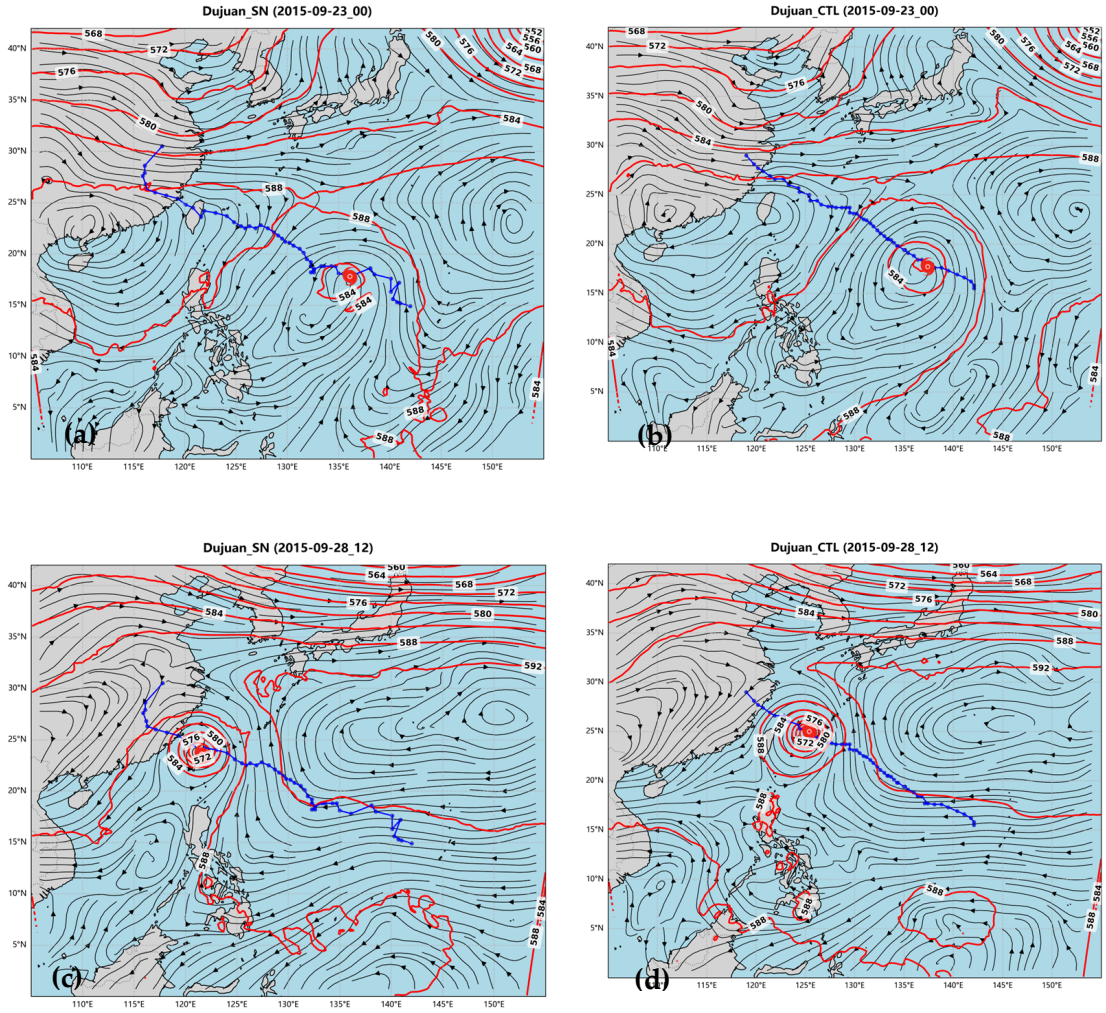


Figure 7. The 500 hPa streamlines for Dujuan (2015) simulated by SN (**a**,**c**) and CTL (**b**,**d**) at 0000 UTC, 23 September 2015, and 1200 UTC, 28 September 2015, respectively. The red symbol marks the storm center.

4.4. Westward Track Passing South of Taiwan

Type 3 track patterns, characterized by westward storm movement south of Taiwan, were largely influenced by westward zonal steering flow to the south of the subtropical high-pressure system over the WNP and the South China Sea (SCS). Under such zonal steering conditions, most CTL simulations produced relatively small lateral (cross-track) track errors (Figure 8). However, the TPEs for the CTL runs remained substantial, ranging from 112.85 km (Typhoon Damrey) to 361 km (Typhoon Utor) (Table 3), suggesting along-track TPE resulting from storm translation speed errors was a significant part of the total TPE.

CTL simulations of Haiyan (2013) and Rammasun (2014) also produced visible lateral track errors (Figure 8). For Haiyan, CTL experiments depicted a weaker circulation over the TC at 500 hPa and a diminishing steering influence from the subtropical high, resulting in a southward deflection of the simulated track (Figure 9a,b). For Rammasun, CTL runs distorted the large-scale environmental flow, causing significant track errors (Figure 9c,d). Spectral nudging was quite effective in reducing both lateral and along-track TPEs. Overall, SN simulations reduced the TPE by a staggering 77% on average.

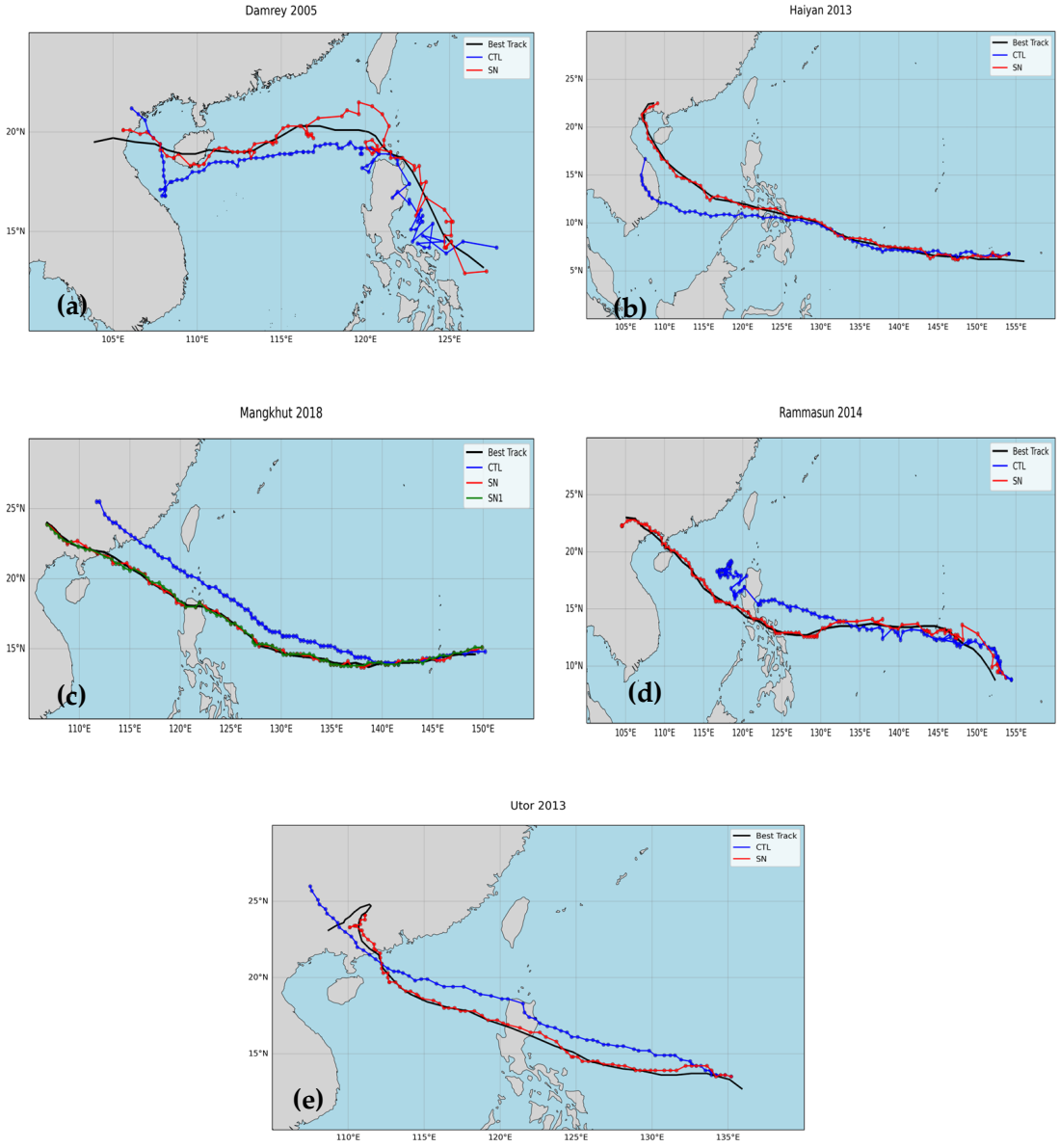


Figure 8. Simulated storm tracks of Type 3 TCs for CTL and SN runs. Black curves represent the best track, blue curves represent CTL, and red and green curves represent SN and SN1, respectively. (**a**–**e**) Darmey (2005), Haiyan (2013), Mangkut (2018), Rammasun (2018), and Utor (2013), respectively.

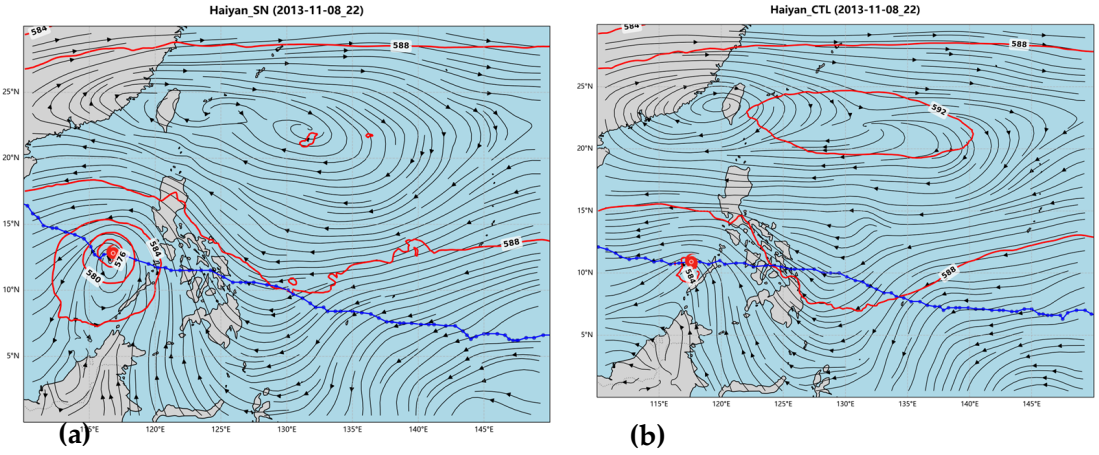


Figure 9. *Cont.*

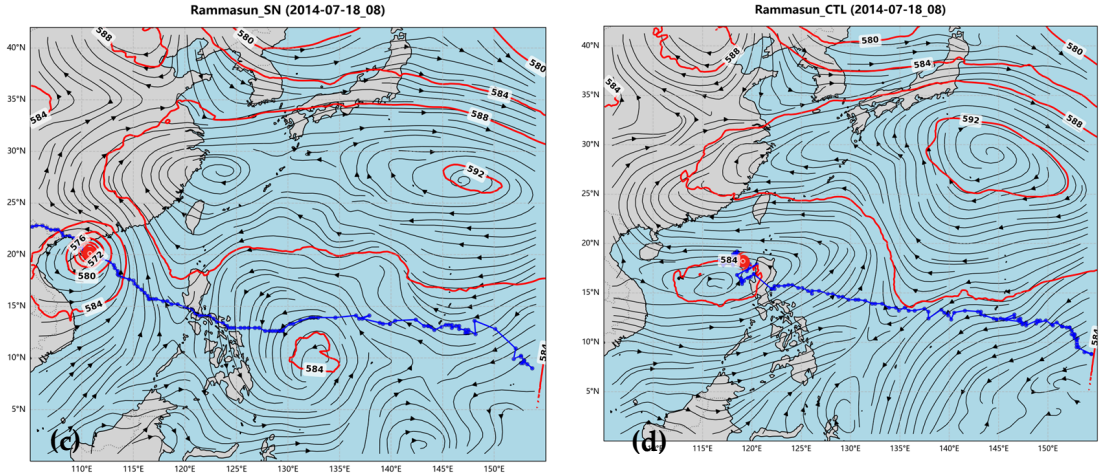


Figure 9. The 500 hPa streamlines for Haiyan (2013) simulated by SN (**a**) and CTL (**b**) at 2200 UTC, 8 November 2013, and Rammasun (2014) simulated by SN (**c**) and CTL (**d**) at 0800 UTC, 18 July 2014. The red symbol marks the storm center.

4.5. Irregular Track

Irregular (Type 4) tracks frequently occur over the SCS [21]. In these cases, CTL simulations produced larger track errors (Figure 10). The steering flow in irregular tracks was often weak due to the distant subtropical high or interactions with multiple circulation systems. Additionally, the complex geography of the SCS contributed to track irregularities.

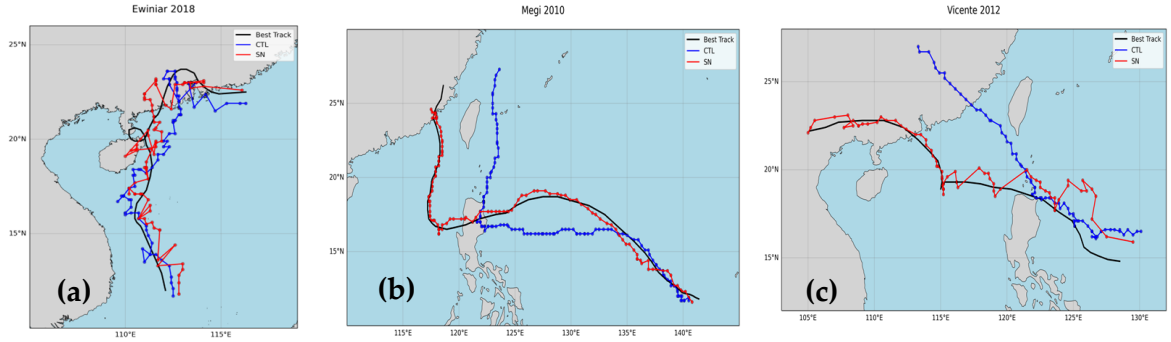


Figure 10. Simulated storm tracks of Type 4 TCs for CTL and SN runs. Black curves represent the best track, blue curves represent CTL, and red curves represent SN. (**a**–**c**) Ewiniar (2018), Megi (2010), and Vincente (2012), respectively.

While SN simulations improved large-scale flow representation, irregular tracks were also influenced by small- and regional-scale systems, such as mesoscale convective systems, as well as coastal terrain. Therefore, SN runs produced mixed results in improving the simulated tracks. While SN was effective for Megi (2010) and Vincente (2012), with 74.8% and 58.4% TPE reduction, respectively, it was not effective for Ewiniar (2018). For Typhoon Ewiniar (2018), SN led to an approximate 20% increase in mean absolute track errors (Table 3) as the storm wandered near the coast (Figure 10a).

5. Conclusions and Discussions

Accurate tropical cyclone (TC) track forecasts provide critical information for disaster prevention and mitigation efforts. In this study, the effectiveness of the spectral nudging technique in simulating four types of TC track patterns (curving, northwestward, westward, and irregular tracks) over the WNP was evaluated using the Weather Research and Forecasting (WRF) model. The results indicate that overall, the spectral nudging technique

demonstrated remarkable effectiveness for all types of regular TC track patterns (Type 1–3), achieving TPE reductions of approximately 60%, 67%, and 77% on average for northward-curving (Type 1), northwestward (Type 2), and westward (Type 3) tracks, respectively.

Type 4 tracks, which are characterized by irregular TC movement over the South China Sea (SCS), presented additional challenges for track forecasters. Weak steering flows, mesoscale convective systems, and complex coastal terrain introduced greater uncertainty in track forecasts. Under these conditions, the spectral nudging technique produced mixed results, highlighting the uncertainties of the SN technique in capturing the influence of regional-scale circulation and local terrain-related factors on irregular TC tracks.

It is important to note that while spectral nudging can improve tropical cyclone track forecasts under certain scenarios by introducing an additional nudging term to the nudging variable tendency equations, it does not represent any new physics. Instead, it primarily serves to constrain large-scale variables toward better alignment with outer-domain analysis or forecasts.

As a final note, although this study focuses on TC tracks, spectral nudging also improves TC intensity simulations. For typhoon intensity, out of the 29 typhoon cases studied, 19 (approximately 66%) exhibited a reduction in intensity error (the absolute error of the maximum wind speed near the TC center) in the SN runs compared with the CTL runs as a result of the smaller track errors simulated by the SN runs. Since higher resolutions are generally needed to accurately simulate TC intensity, more studies with higher grid resolutions are needed to quantitatively assess the impact of the spectral nudging technique on TC intensity simulations and forecasts.

Author Contributions: Conceptualization, W.H. and L.X.; methodology, W.H. and L.X.; software, W.H., L.X., F.H. and J.Z.; validation, W.H. and L.X.; formal analysis, W.H. and L.X.; investigation, W.H., L.X., F.H. and J.Z.; resources, L.X.; data curation, W.H., L.X., F.H. and J.Z.; writing—original draft preparation, W.H.; writing—review and editing, L.X.; visualization, W.H., F.H. and J.Z.; supervision, L.X.; project administration, L.X.; funding acquisition, L.X. and W.H. All authors have read and agreed to the published version of the manuscript.

Funding: This project was partially supported by Lenovo through a gift to North Carolina State University and by the Key Innovative Research Program of HuaFeng Meteorological Media Group (grant No. CY-2023ZDIAN03) during the final preparation and publication of this manuscript.

Institutional Review Board Statement: Not applicable.

Informed Consent Statement: Not applicable.

Data Availability Statement: The raw data supporting the conclusions of this article will be made available by the authors on request.

Acknowledgments: W.H. acknowledges the support by the China Meteorological Administration and the China Scholarship Council during her scholarly visit to North Carolina State University.

Conflicts of Interest: Author Weiwei Huang, Fei Hong and Jiwen Zhu were employed by the company Beijing Fengyun Meteorological Science and Technology Development Co., Ltd. The remaining author declares that the research was conducted in the absence of any commercial or financial relationships that could be construed as a potential conflict of interest.

Abbreviations

The following abbreviations are used in this manuscript:

SCS	South China Sea
WNP	Western North Pacific
TC	Tropical cyclone

CTL	Control sensitivity experiment
SN	Spectral nudging sensitivity experiment

References

1. Elsner, J.B.; Liu, K.-B. Examining the ENSO-typhoon hypothesis. *Clim. Res.* **2003**, *25*, 43–54. [CrossRef]
2. Chen, L. Tropical meteorological calamities and its research evaluation. *Meteorol. Mon.* **2010**, *36*, 101–110.
3. Schmidt, S.; Kemfert, C.; Höppe, P. The impact of socio-economics and climate change on tropical cyclone losses in the USA. *Reg. Environ. Change* **2010**, *10*, 13–26. [CrossRef]
4. Wei, Z.; Sui, G.; Tang, D. An overview of assessment and approaches on typhoon disaster. *J. Catastrophol.* **2012**, *27*, 117–123.
5. Huang, W.; Duan, Y.; Xue, J.; Chen, D. Operational experiments and its performance analysis of the tropical cyclone numerical model (GRAPES_TCM). *Acta Meteorol. Sin.* **2007**, *65*, 578–587.
6. Goerss, J.S.; Sampson, C.R. A history of Western North Pacific tropical cyclone track forecast skill. *Weather Forecast.* **2004**, *19*, 633–638. [CrossRef]
7. Yamaguchi, M.; Ishida, J.; Sato, H.; Nakagawa, M. WGNE intercomparison of tropical cyclone forecasts by opertional NWP models: A quarter century and beyond. *Bull. Am. Meteorol. Soc.* **2017**, *98*, 2337–2349. [CrossRef]
8. Chan, J.C.L.; Gary, W.M. Tropical cyclone movement and surrounding flow relationships. *Mon. Weather Rev.* **1982**, *110*, 1354–1374. [CrossRef]
9. Xie, L.; Liu, B.; Peng, S. Application of scale-selective data assimilation to tropical cyclone track simulation. *J. Geophys. Res.* **2010**, *115*, D17105. [CrossRef]
10. Waldron, K.M.; Paegle, J.; Horel, J.D. Sensitivity of a spectrally filtered and nudged limited-area model to outer model options. *Mon. Weather Rev.* **1996**, *124*, 529–547.
11. von Storch, H.; Langenberg, H.; Feser, F. A spectral nudging technique for dynamical downscaling purposes. *Mon. Weather Rev.* **2000**, *128*, 3664–3673. [CrossRef]
12. Miguez-Macho, G.; Stenchikov, G.L.; Robock, A. Regional climate simulations over North America: Interaction of local processes with improved large-scale flow. *J. Clim.* **2005**, *18*, 1227–1246. [CrossRef]
13. Liu, B.; Xie, L. A scale-selective data assimilation approach to improving tropical cyclone track and intensity forecasts in a limited-area model: A case study of hurricane Felix (2007). *Weather Forecast.* **2012**, *27*, 124–140. [CrossRef]
14. Cha, D.; Wang, Y. A dynamical initialization scheme for real-time forecasts of tropical cyclones using the WRF model. *Mon. Weather Rev.* **2013**, *141*, 964–986. [CrossRef]
15. Guo, X.; Zhong, W. The use of a spectral nudging technique to determine the impact of environmental factors on the track of typhoon Megi (2010). *Atmosphere* **2017**, *8*, 257. [CrossRef]
16. Qu, H.; Li, X.; Ling, T.; Zhang, Y. Influence of spectral nudging assimilation technique on typhoon track and intensity simulation. *Mar. Forecast.* **2018**, *35*, 17–29.
17. Skamarock, W.C.; Klemp, J.B.; Dudhia, J.; Gill, D.O.; Liu, Z.; Berner, J.; Wang, W.; Powers, J.G.; Duda, M.G.; Barker, D.M.; et al. A description of the Advanced Research WRF Model version 4. In *NCAR Technical Notes NCAR/TN-556+STR*; National Center Atmospheric Research: Boulder, CO, USA, 2019.
18. Ying, M.; Zhang, W.; Yu, H.; Lu, X.; Feng, J.; Fan, Y.; Zhu, Y.; Chen, D. An overview of the China Meteorological Administration tropical database. *J. Atmos. Oceanic Technol.* **2014**, *31*, 287–301. [CrossRef]
19. Mann, H.B.; Whitney, D.R. R. On a test of whether one of two random variables is stochastically larger than the other. *Ann. Math. Stat.* **1947**, *18*, 50–60. [CrossRef]
20. Huang, W.; Dong, J.; Wang, J.; Xu, Y. Characteristics of extratropical transition of hurricane Sandy. *J. Meteorol. Environ.* **2015**, *31*, 53–62.
21. Yu, J.; Tang, J.; Dai, Y.; Yu, B. Analyses in errors and their causes of Chinese typhoon track operational forecasts. *Meteorol. Mon.* **2012**, *38*, 695–700.

Disclaimer/Publisher's Note: The statements, opinions and data contained in all publications are solely those of the individual author(s) and contributor(s) and not of MDPI and/or the editor(s). MDPI and/or the editor(s) disclaim responsibility for any injury to people or property resulting from any ideas, methods, instructions or products referred to in the content.